URSI GASS 2021, Rome, Italy, 28 August - 4 September 2021

Spectral index of the Galactic foreground emission in the 50-87 MHz range with LEDA

M. Spinelli*[(1)(2)], G. Bernardi[(3)(4)(5)], H. Garsden[(6)], L.J. Greenhill[(7)], A. Fialkov[(8)(9)], J. Dowell[(10)] and D.C. Price[(7)(11)]
(1) INAF-Osservatorio Astronomico di Trieste, Via G.B. Tiepolo 11, 34143 Trieste, Italy
(2) IFPU - Institute for Fundamental Physics of the Universe, Via Beirut 2, 34014 Trieste, Italy
(3) INAF-Istituto di Radioastronomia, via Gobetti 101, 40129, Bologna, Italy
(4) Department of Physics & Electronics, Artillery Road, Rhodes University, Grahamstown, South Africa
(5) South African Radio Astronomy Observatory, FIR street, Observatory, Cape Town, South Africa
(6) Queen Mary University of London, Mile End Rd, Bethnal Green, London E1 4NS, UK
(7) Center for Astrophysics, Harvard & Smithsonian, 60 Garden Street, Cambridge MA 02138 USA
(8) Kavli Institute for Cosmology, Madingley Road, Cambridge CB3 0HA, UK
(9) Institute of Astronomy, University of Cambridge, Madingley Road, Cambridge CB3 0HA, UK
(10) University of New Mexico, 1919 Lomas Boulevard NE, Albuquerque, NM 87131, USA
(11) International Centre for Radio Astronomy Research, Curtin University, Bentley WA 6102, Australia

Abstract

Total power radiometry with individual meter-wave antennas is a potentially effective means to detect the brightness temperature from the 21 cm line of neutral hydrogen during the Cosmic Dawn. In the process, spectra of integrated sky brightness temperature can be used to quantify properties of foreground emission. In this work we analyze a subset of data from the Large-aperture Experiment to Detect the Dark Age (LEDA) and constrain the spectral index β of foreground emission in the northern sky. We correct for the effect of gain pattern chromaticity and compare estimated absolute temperatures with simulations. We estimate variation in β with local sidereal time (LST) using two widely spaced, zenith-directed radiometers during May and December 2018, and January-May 2019. For times in the 9-12.5h LST window when the Sun is not in the Sky and the Galactic Center is at least 20° below the local horizon, we estimate $\beta = -2.48 \pm 0.07$ for the first antenna, and $\beta = -2.57 \pm 0.12$ for the second. These results are consistent with previous measurements of the southern sky. Anomalously heavy rainstorms moved through the observing site in winter 2019. The coincident timing of episodic shifts in the temperature scales of the two radiometers suggests substantial sensitivity to the the changes in the soil moisture profile, though other variables may also be involved. We extend the analysis December/January data, for which soil conditions are optimal, to an almost 24 h LST range finding results in agreement with simulated sky models.

1 Introduction

The challenging measurement of a signal from the Cosmic Dawn of the Universe finds its most promising observable in the 21 cm line of the neutral Hydrogen. The interplay between Ly-α coupling and X-ray heating is thus expected to create a few hundreds mK absorption features in the *global - i.e. sky averaged* - 21 cm signal, sensitive to the formation of the first luminous structures in the Universe and to the thermal history of the intergalactic medium. The key challenge to measuring the 21 cm signal is the subtraction of the bright foregrounds. Global signal experiments, while targeting the Cosmic Dawn, can contribute to the knowledge of the low-frequency radio sky: with their large beams they average the absolute sky brightness temperature over large spatial scales. The diffuse and continuum foreground sources are known to be spectrally smooth; that is, they should exhibit power-law spectra[1] over the low frequency band of interest. Measurements of the Galactic foreground spectral index β have been obtained with single dipole antennas. [1] found, for the frequency range $100-200$ MHz, that the spectral index of diffuse emission was $\beta = -2.5 \pm 0.1$ at high-Galactic latitudes. [2], using the SARAS experiment, measured the spectral index in the $110-170$ MHz band covering the $23-1$ h local sidereal time (LST) range. They reported a slow variation with LST and a steepening from -2.3 to -2.45 when observing off the Galactic center. In [3], the EDGES team obtained a measurement of the spectral index in the southern hemisphere, in the frequency range $90-190$ MHz. They found $-2.60 > \beta > -2.62$ in the $0-12$ h LST range, with an increase up to $\beta = -2.50$ at 17.7 h, when the Galactic center is transiting. In the $50-100$ MHz range, [4] found the spectral index to be $-2.59 < \beta < -2.54$ for LST values below 12 h and a flattening to -2.46 when the Galactic center transits.

The LEDA experiment covers instead the full northern hemisphere, offering an important complementary measure of the spectral index. [5], using LEDA data from 40 to 83 MHz, found that the spectral index varies between -2.28 to -2.38 over the full LST range. In this work,

[1] $T(\nu) \propto \nu^{\beta}$

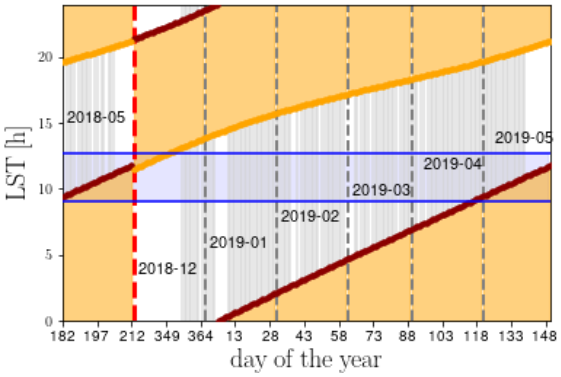

Figure 1. The distribution, between May 2018 and May 2019, of the 137 nights analyzed in this work (gray vertical solid lines). The yellow band indicates the daylight, defined between sunrise (orange line) and sunset (dark red line). Dashed vertical lines divide the months. Note there is a gap between May 2018 and December 2018 highlighted with a red thick dashed line. The horizontal blue strip highlight the ~ 4 hours LST range main focus of our analysis.

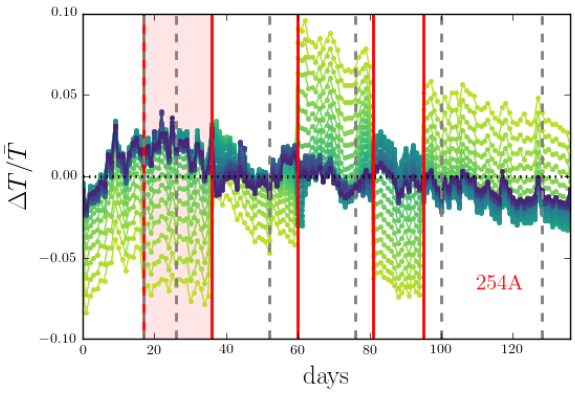

Figure 2. Variations of the measured sky temperature, for 1 h integration time around LST = 12 h, as a function of observing day, for antenna 254A. We plot the relative difference with respect to its mean value $\bar{T}$. Different colors indicate different frequencies: lower (higher) frequencies are shown in lighter greens (darker blues). Dashed vertical lines denote the separation between months as for Figure 1. The relative temperature discontinuities are common to both antennas and are highlighted in the plot with red vertical lines and define the six different *datasets*. Our *reference* dataset are December 2018 and January 2019, marked as a red shaded region.

we present new results on the spectral index of the Galactic foreground emission in the $50-87$ MHz range using the latest LEDA measurements, covering ~ 140 nights distributed between mid-2018 to mid-2019.

2 Observations and data processing

Detailed descriptions of LEDA systems can be found in [6] and [5]. LEDA dual polarization radiometric receivers were installed in place of LWA receivers on a subset of antennas within the OVRO-LWA (37° 14′ 23.1998" N, 118° 16′ 53.9995" W). In this analysis we report on results using the east-west dipole (polarization A) from antennas 252 and 254. Antenna 254 was equipped with a 3 m × 3 m ground screen, the default for the OVRO LWA station. Through January 2019, the same applied to antenna 252. Afterward, the small screen was replaced by a 20 m × 20 m ground screen. The Galactic plane contributes significantly to the overall system temperature of zenith-directed low-frequency radiometers, so, for aiming at a detection of the 21 cm signal, it is better to observe when the brightest portions of the plane are low in the sky. We report in Figure 1 the preferred LST range for our analysis ($9-12.5$ h LST), which combines low Galactic plane contribution and night hours across all the observing period.

We averaged the signal over 1 MHz-wide channels, using the variance computed in each channel as a weight. The typical noise in a 1 MHz channel is a few Kelvin at 75 MHz for a 5 s integration time. These 1 MHz spectra are the ones used in our analysis.

The measured temperature varies as a function of LST as the foreground sky changes as observed by a fixed antenna, however, it is ideally the same if measured at the same LST over different days. Figure 2 shows how the observed temperature varies over the course of our observations. Temporal variations are frequency-dependent in both antennas, with larger effects at low frequencies. We mark them in the Figure with red vertical lines and define in this way six different *datasets*, where temperature remains fairly constant with time. The time discontinuities appear more evident in antenna 252A (not reported in the Figure) although contained at few % level, reaching $10-20\%$ only at the lowest frequencies ($\nu < 60$ MHz).

The consistency of low-frequency radiometer performance depends in part on the environment: seasonal dry conditions in 2018 carrying over from summer persisted into the first half of January 2019. Consequently, the data acquired in December 2018 and January 2019 are defined our *reference* dataset.

We then study the variation over time of the spectra measured by the two antennas. We show in Figure 3 the relative difference with respect to the mean value $\bar{T}$, computed by averaging all measured spectra. We plot the six *datasets* defined above with different colors. The 254A data show good stability; for frequencies higher than 60 MHz, within-datasets and between-datasets differences are at most 5% and do not evolve much with frequency. Below 60 MHz, the different trends highlighted in Figure 2 are again clearly visible, leading to differences up to 10%. Antenna 252A (not reported in the Figure) has good consistency within each dataset, while differences across datasets can be as high as 30%. These latter are due both to temporal offsets as

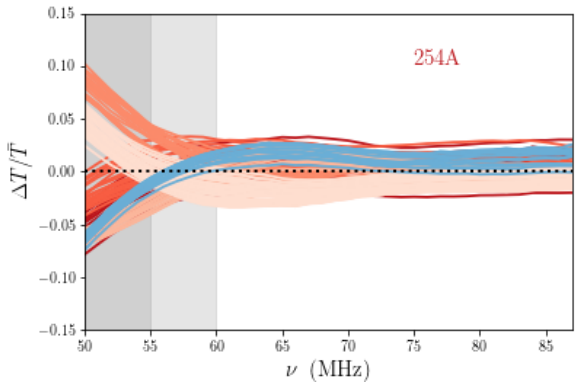

Figure 3. Time variation of the sky spectra measured by antenna 254A, plotted as the relative difference with respect the mean value $\bar{T}$ - each color is a different *dataset* as defined in Figure 2. Chronologically earlier (later) datasets are shown in darker (lighter) colors. The *reference* dataset appears in blue in both plots in order to facilitate its identification. Gray shaded areas identify the lowest frequencies (dark gray $\nu < 55$ MHz, light gray $\nu < 60$ MHz).

well as low frequency variations. Differences are smaller at higher frequencies. We note that antenna 252A has a particularly marked discontinuity between January and February, corresponding to maintenance activities.

The spectral smoothness of the foreground emission is the key property that should allow the retrieval of the 21 cm signal. Regardless of the parametrization used for the foregrounds, a frequency-dependent response of the antenna could corrupt their intrinsic spectra and thus prevent the extraction of the global signal. Observed spectra were corrected for the effect of beam chromaticity following [3, 4] and re-scaled to be in agreement with the absolute temperature scale derived from existing observations of [7, 8]. The beam chromaticity effect leads to spectral index corrections of no more than $\sim 4\%$. We note here that an approach that incorporates beam effects in the foreground model and, therefore, bypasses the chromaticity correction, has recently been discussed in the literature [9, 10], although not applied to observations yet.

3 Results

We analyze our observations to characterize the spectral index of the foreground emission. We concentrate on the $9-12.5$ h LST range, that corresponds to the minimum of foreground contamination. Note that this LST range is the central interval of interest for further studies aimed at extracting a global signal constraint/upper limit.
We model the data with a simple power law.
Following [4] we write

$$T_{\rm m}(\nu;\beta,{\rm T}_{75}) = {\rm T}_{75}\left(\frac{\nu}{\nu_{75}}\right)^{\beta} + T_{\rm cmb}, \qquad (1)$$

Table 1. Mean of the best-fit spectral index β (equation 1) for each of the six *dataset*s, obtained by averaging over the LST range $9-12.5$ h. The quoted RMS values are averaged accordingly. The errors $\Delta\beta$ are computed from the standard deviation of the spectra.

	254 A			252 A		
dset	β	$\Delta\beta$	rms (K)	β	$\Delta\beta$	rms (K)
1	-2.47	0.01	19.32	-2.39	0.01	48.72
2 (*ref*)	-2.54	0.03	21.60	-2.47	0.10	44.88
3	-2.50	0.06	24.15	-2.66	0.09	52.86
4	-2.44	0.06	25.35	-2.63	0.08	60.20
5	-2.45	0.06	23.90	-2.65	0.09	58.11
6	-2.41	0.02	25.88	-2.58	0.02	59.30

choosing 75 MHz as a reference frequency and considering spectra only above 60 MHz.
We perform a χ^2 minimization to constrain the model parameters for each LST bin and we report in Table 1 the mean and standard deviation for each dataset. We also report the averaged RMS values of the residuals.

The distribution of the best fit spectral indexes for antenna 254A spans values from -2.54 to -2.41, all consistent with the mean $\beta = -2.48 \pm 0.07$. Spectral index are in general less stable for antenna 252A, leading to a mean value $\beta = -2.57 \pm 0.12$, all consistent, however, with the values from 254A within the 2σ confidence interval. The best-fit values of T_{75} are not reported but we remark their agreement with the (offset corrected) measured value of the sky temperature at 75 MHz.

We focus then on our *reference* dataset whose observing conditions are optimal in terms of soil and rainfall. We study the spectral index averaging the spectra in LST bins of 5 minutes and extend the analysis to daytime data allowing us to consistently analyze an almost 24 h LST range. The Sun is a potential source of interference, especially during flare events. Nevertheless, our daytime spectra do not show any features or non-smooth variations and we checked that the Sun was mostly quite during our observing time using data from the Learmonth Solar Radio Spectrograph[2]. Moreover, we estimate the beam weighted contribution of the quiet sun at transit in December/January using [11] to be 35 K at 80 MHz, i.e. a $\sim 1\%$ contribution to the total sky temperature. We find that the spectral index is fairly flat across 24 h LST range. It varies from $\beta = -2.55 \pm 0.01$ for antenna 254A at LST < 6 h to $\beta = -2.58 \pm 0.01$ at LST ~ 13 h. A similar behavior is found for antenna 252A, although with a flatter mean spectral index, changing from $\beta = -2.43 \pm 0.02$ to $\beta = -2.46 \pm 0.02$. Residual rms values after subtracting the best fit power law vary from $20-30$ K for antenna 254A to $70-150$ K for antenna 252A. The combined result of the two antennas is shown in the lower panel of Figure 4.

[2] https://www.sws.bom.gov.au/

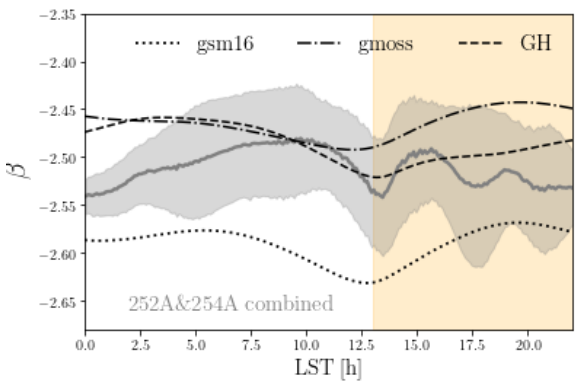

Figure 4. Mean value of the best fit daily spectral index β, as a function of LST, obtained for the beam corrected *reference* dataset when combining the two antennas (solid gray line) and its scatter (shaded area). The result compared with the Guzman-Haslam (black dashed), improved GSM (black dotted) and GMOSS (black dashed dotted) spectral index (see text for details). For illustrative purposes, the shaded yellow area indicates daylight, starting approximately from sunrise.

Our result is consistent with previous measurements. [7] derived a spectral index map from 45 MHz and 408 MHz with $-2.6 < \beta < -2.5$ over most of the sky. Similarly, [4] found $-2.59 < \beta < -2.54$ at LSTs from 0 to 12 h in the $50-100$ MHz range, flattening to $\beta = -2.46$ when the Galactic center is transiting - although their observations cover the southern celestial hemisphere and can, therefore, only be qualitatively compared to ours. Moreover, we find broad agreement with the Improved GSM [12] and GMOSS [13] sky models.

4 Acknowledgements

The authors kindly thank the Caltech OVRO staff for the great dedication and skills demonstrated in constructing the LWA array. MS acknowledges funding from the INAF PRIN-SKA 2017 project 1.05.01.88.04 (FORECaST) and support from the INFN INDARK PD51 grant. AF is supported by the Royal Society University Research Fellowship. LEDA research has been supported in part by NSF grants AST/1106059, PHY/0835713, and OIA/1125087. The OVRO-LWA project was enabled by the kind donation of Deborah Castleman and Harold Rosen.

References

[1] A. Rogers and J. Bowman, "Spectral index of the diffuse radio background measured from 100 to 200 mhz," *Astron. J.*, vol. 136, 06 2008.

[2] N. Patra, R. Subrahmanyan, S. Sethi, N. U. Shankar, and A. Raghunathan, "SARAS MEASUREMENT OF THE RADIO BACKGROUND AT LONG WAVELENGTHS," *The Astrophysical Journal*, vol. 801, p. 138, mar 2015.

[3] T. J. Mozdzen, J. D. Bowman, R. A. Monsalve, and A. E. E. Rogers, "Improved measurement of the spectral index of the diffuse radio background between 90 and 190 MHz," , vol. 464, pp. 4995–5002, Feb. 2017.

[4] T. J. Mozdzen, N. Mahesh, R. A. Monsalve, A. E. E. Rogers, and J. D. Bowman, "Spectral index of the diffuse radio background between 50 and 100 MHz," , vol. 483, pp. 4411–4423, Mar. 2019.

[5] D. C. Price et al., "Design and characterization of the Large-aperture Experiment to Detect the Dark Age (LEDA) radiometer systems," , vol. 478, pp. 4193–4213, Aug. 2018.

[6] J. Kocz and L. J. Greenhill et al., "Digital Signal Processing Using Stream High Performance Computing: A 512-Input Broadband Correlator for Radio Astronomy," *Journal of Astronomical Instrumentation*, vol. 4, p. 1550003, June 2015.

[7] A. E. Guzmán, J. May, H. Alvarez, and K. Maeda, "All-sky Galactic radiation at 45 MHz and spectral index between 45 and 408 MHz," , vol. 525, p. A138, Jan. 2011.

[8] C. G. T. Haslam, C. J. Salter, H. Stoffel, and W. E. Wilson, "A 408 MHz all-sky continuum survey. II. The atlas of contour maps.," , vol. 47, pp. 1–143, Jan. 1982.

[9] K. Tauscher, D. Rapetti, and J. O. Burns, "Formulating and Critically Examining the Assumptions of Global 21 cm Signal Analyses: How to Avoid the False Troughs That Can Appear in Single-spectrum Fits," , vol. 897, p. 132, July 2020.

[10] D. Anstey, E. de Lera Acedo, and W. Handley, "A General Bayesian Framework for Foreground Modelling and Chromaticity Correction for Global 21cm Experiments," *arXiv e-prints*, p. arXiv:2010.09644, Oct. 2020.

[11] A. O. Benz, "Radio Emission of the Quiet Sun," *Landolt Börnstein*, vol. 4B, p. 103, Jan. 2009.

[12] H. Zheng, M. Tegmark, J. S. Dillon, D. A. Kim, A. Liu, A. R. Neben, J. Jonas, P. Reich, and W. Reich, "An improved model of diffuse galactic radio emission from 10 MHz to 5 THz," *Monthly Notices of the Royal Astronomical Society*, vol. 464, pp. 3486–3497, 10 2016.

[13] M. Sathyanarayana Rao, R. Subrahmanyan, N. Udaya Shankar, and J. Chluba, "GMOSS: All-sky Model of Spectral Radio Brightness Based on Physical Components and Associated Radiative Processes," , vol. 153, p. 26, Jan. 2017.